High-Temperature Catalysts for the Production of α-Olefins Based on Iron(II) and Cobalt(II) Tridentate Bis(imino)pyridine Complexes with a Double Pattern of Substitution: *o*-Methyl plus *o*-Fluorine in the Same Imino Arm†

Alex S. Ionkin,* William J. Marshall, Douglas J. Adelman, Barbara Bobik Fones, Brian M. Fish, and Matthew F. Schiffhauer

DuPont Central Research & Development, Experimental Station, Wilmington, Delaware 19880-0328

Rupert E. Spence and Tuyu Xie

E. I. du Pont Canada Company, Research and Development Center, Kingston, Ontario, Canada K7L 5A5

Received November 30, 2007

The new series of bis(imino)pyridine ligands [2-F-6-MePhN═C(Me)PyC(Me)═NPh-2-F-6-Me] (**14**), [2-F-6-MePhN═C(Me)PyC(Me)═NPh-2-Me] (**19**), and [2-F-6-MePhN═C(Me)PyC(Me)═N-Ph-2,4-Me_2] (**20**) and their corresponding Fe(II) complexes [{2-F-6-Me-PhN═C(Me)PyC(Me)═NPh-2-F-6-Me}$FeCl_2$] (**4**), [{2-F-6-MePhN═C(Me)PyC(Me)═NPh-2-Me}$FeCl_2$] (**5**), and {[2-F-6-MePhN═C(Me)PyC(Me)═NPh-2,4-Me_2]$FeCl_2$} (**6**) and Co(II) complex [{2-F-6-MePhN═C(Me)PyC(Me)═NPh-2-Me}CoI_2] (**7**) with a double pattern of substitution, *o*-methyl plus *o*-fluorine in the same imino arm, were synthesized and fully characterized. According to X-ray analysis **4**, **5**, and **7** exist mostly in the unexpected "up-up" conformers in the solid state. The Co−N bonds in **7** are shorter than the corresponding Fe−N bonds in the analogous complex **5** by 0.003−0.025 Å. This shortening of metal−N bonds going from iron(II) to cobalt(II) complexes can be explained by the smaller van der Waals radius of Co vs. that of Fe. The Fe complexes **4**–**6** afforded very productive catalysts for the production of α-olefins with a more linear Schultz−Flory distribution of α-olefins and with higher *K* values than the parent methyl-substituted Fe(II) complex [{2-MePhN═C(Me)PyC(Me)═NPh-2-Me}$FeCl_2$] (**1**). The cobalt complex **7** was found to have very low activity in α-olefin oligomerization experiments within the tested range of temperatures (60–130 °C).

Introduction

Fe^{II} catalysts with tridentate bis(imino)pyridine ligands were reported to make α-olefin oligomers with perfect Schultz−Flory distributions, in exceptional purities (97–99%), and with high productivities.[1a] The results exceed the values reported for catalysts used in the current commercial processes, including the original Ziegler process and Shell's SHOP technology.[2] The presence of sterically small substituents in the ortho positions of the imino aryl group, such as only one methyl group in the ortho positions in complex **1** or the fluorides in the ortho positions in complex **2** (Scheme 1), are crucial catalyst structural features needed to produce just α-olefins instead of polyethylene.[1,3] The combination of *o*-fluorine and *o*-trifluoromethyl substituents, for example in complex **3**, was found to enhance the catalytic performance.[4a]

The Fe^{II} complex **1** with a tridentate bis(imino)pyridine ligand, bearing only one methyl group in the ortho positions of the imino aryl group, was initially determined to be the best for α-olefin production.[1c,e] However, thorough analysis of complex **1** as a precatalyst for α-olefin oligomerization at the commercially desirable temperature of 120 °C revealed some

* To whom correspondence should be addressed. E-mail: alex.s.ionkin@usa.dupont.com.

† This is DuPont Contribution No. 8701.

(1) For initial publications, see: (a) Bennett, A. M. A. (DuPont). *PCT Int. Appl. WO9827124 A1*, 1998. (b) Britovsek, G. J. P.; Gibson, V. C.; Kimberley, B. S.; Maddox, P. J.; McTavish, S. J.; Solan, G. A.; White, A. J. P.; Williams, D. J. *Chem. Commun.* **1998**, 849. (c) Small, B. L.; Brookhart, M. *J. Am. Chem. Soc.* **1998**, *120*, 7143. For recent reviews and papers, see: (d) Ittel, S. D.; Johnson, L. K.; Brookhart, M. *Chem. Rev.* **2000**, *100*, 1169. (e) Britovsek, G. J. P.; Gibson, V. C.; Wass, D. F. *Angew. Chem., Int. Ed.* **1999**, *38*, 428. (f) Mecking, S. *Coord. Chem. Rev.* **2000**, *203*, 325. (g) Gibson, V. C.; Spitzmesser, S. K. *Chem. Rev.* **2003**, *103*, 283. (h) Britovsek, G. J. P.; Cohen, S. A.; Gibson, V. C.; van Meurs, M. *J. Am. Chem. Soc.* **2004**, *126*, 10701. (i) Barbaro, P.; Bianchini, C.; Giambastiani, G.; Rios, I. G.; Meli, A.; Oberhauser, W.; Segarra, A. M.; Sorace, L.; Toti, A. *Organometallics* **2007**, *26*, 4639. (j) Bart, S. C.; Lobkovsky, E.; Bill, E.; Wieghardt, K.; Chirik, P. J. *Inorg. Chem.* **2007**, *46*, 7055. (k) Abu-Surrah, A. S.; Qaroush, A. K. *Eur. Polym. J.* **2007**, *43*, 2967. (l) Zhang, S.; Vystorop, I.; Tang, Z.; Sun, W.-H. *Organometallics* **2007**, *26*, 2456. (m) Small, B. L.; Rios, R.; Fernandez, E. R.; Carney, M. J. *Organometallics* **2007**, *26*, 1744. (n) McTavish, S.; Britovsek, G. J. P.; Smit, T. M.; Gibson, V. C.; White, A. J. P.; Williams, D. J. *J. Mol. Catal. A: Chem.* **2007**, *261*, 293. (o) Seitz, M.; Milius, W.; Alt, H. G. *J. Mol. Catal. A: Chem.* **2007**, *261*, 246. (p) Kaul, F. A. R.; Puchta, G. T.; Frey, G. D.; Herdtweck, E.; Herrmann, W. A. *Organometallics* **2007**, *26*, 988. (q) Mahdavi, H.; Badiei, A.; Zohuri, G. H.; Rezaee, A.; Jamjah, R.; Ahmadjo, S. J. *Appl. Polym. Sci.* **2007**, *103*, 1517.

(2) Vogt, D. In *Applied Homogeneous Catalysis with Organometallic Compounds*; Cornils, B., Herrmann, W., Eds.; VCH: Weinheim, Germany, 1996; Vol. 1, p 245.

(3) (a) Schmid, M.; Eberhardt, R.; Klinga, M.; Leskela, M.; Rieger, B. *Organometallics* **2001**, *20*, 2321. (b) Moody, L. S.; MacKenzie, P. B.; Killian, C. M.; Lavoie, G. G.; Ponasik, J. A.; Smith, T. W.; Pearson, J. C.; Barrett, A. G. M. *U.S. Pat. Appl., U. S. 2002/0049135 A1*, 2002. (c) Ionkin, A. S.; Marshall, W. J. *Organometallics* **2004**, *23*, 3276. (d) Alt, H. G.; Licht, E. H.; Licht, A. I.; Schneider, K. J. *Coord. Chem. Rev.* **2006**, *250*, 2. (e) Kaul, F. A. R.; Puchta, G. T.; Frey, G. D.; Herdtweck, E.; Herrmann, W. A. *Organometallics* **2007**, *26*, 988.

10.1021/om701204w CCC: $40.75
Publication on Web 02/20/2008

Scheme 1

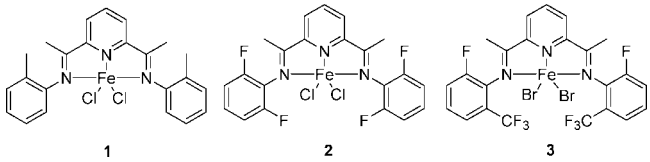

Scheme 2

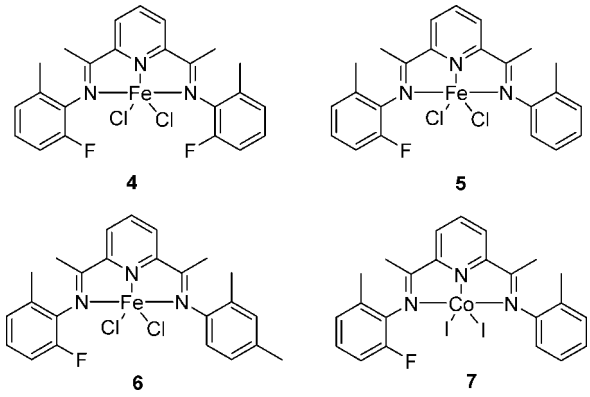

important shortcomings. Complex **1** is extremely productive, but the lifetime of the catalyst is about 3 min at 120 °C. The resulting exothermic effect is difficult to control. Also, the Schulz−Flory distribution is not linear. The distribution was curved, with the light α-olefin fractions (C-4 and C-6) and heavier fractions (C-14 and up) above the theoretical numbers. These challenges needed to be addressed through catalyst modifications.

In this study, we report Fe^{II} and Co^{II} complexes with tridentate bis(imino)pyridine ligands functionalized by the novel combination of *o*-fluorine and *o*-methyl substituents (Scheme 2), which afford high-temperature catalysts for the production of α-olefins. Several patterns of the substitutions were envisioned to make these kinds of complexes that produce just α-olefins. The complex **4** has a symmetrical pattern of substitution in both aryl imino groups. The nonsymmetrical patterns[5] in complexes **5**–**7** have one imino arm with *o*-fluorine and *o*-methyl substituents and in the second imino aryl group have only one *o*-methyl or one *o*-methyl and a *p*-methyl (Scheme 2).

Results and Discussion

Synthesis. The direct ortho-metalation methodology with subsequent functionalization was used to assemble combinations of *o*-fluorine and *o*-methyl substituents in one aryl imino moiety.[6] Thus, commercially available 2-fluorophenylamine (**8**) was protected with a *tert*-butoxycarbonyl (BOC) group to form the corresponding *tert*-butyl 2-fluorophenyl carbamate (**9**) (Scheme 3). Dilithiation of compound **9** by slightly more than 2 equiv of *tert*-butyllithium at low temperature yielded the yellow dianionic species **10**. The reaction between **10** and 1 equiv of methyl iodide, which was followed by hydrolysis, afforded *tert*-butyl 2-fluoro-6-methylphenyl carbamate (**11**). The deprotection of the BOC group was achieved by treating **11** with trifluoroacetic acid to get the formation of target 2-fluoro-6-methylphenylamine (**12**).[7]

The condensation reaction between 2-fluoro-6-methylphenylamine (**12**) and commercially available 1-(6-acetylpyridin-2-yl)ethanone (**13**) led to a symmetrical bis(imino)pyridine (**14**) with the combination of *o*-fluorine and *o*-methyl substituents in one aryl imino moiety. The reaction between iron(II) chloride and ligand **14** led to the complex **4** (Scheme 4).

The structure of complex **4** was determined by X-ray analysis. A crystal of **4** suitable for X-ray analysis was grown from methylene chloride (Figure 1). It should be noted that *o*-fluorine and *o*-methyl substituents adopt an up–up or mutually syn conformation.[4]

Nonsymmetrical complexes of types **5**–**7** were prepared by the following methods. Two sets of selective condensations were used to prepare the ligands for **5**–**7**. The first condensation reactions between commercially available 1-(6-acetylpyridin-2-yl)ethanone (**13**) and *o*-tolylamine (**15**) and 2,4-dimethylphenylamine (**16**) led to the nonsymmetrical (imino)(keto)pyridines **17** and **18**, respectively. The second set of selective condensations between precursors **17** and **18** from one side and the aniline **12** from the other side led to the formation of the target ligands **19** and **20** (Scheme 5).

The reactions between the nonsymmetrical ligands **19** and **20** and iron(II) chloride in THF afforded the final Fe(II) complexes of **5** and **6**. The reaction between cobalt(II) iodide and the ligand **19** afforded the cobalt analogue **7** (Scheme 6).

According to X-ray analysis, complex **6** exists also as an up–up or mutually syn conformer (Figure 2).

Solid-State Structures of Fe Precatalysts. Complexes **4** and **5** have a distorted-bipyramidal geometry, which is typical for iron(II) complexes with tridentate bis(imino)pyridine ligands in a 1:1 ratio.[1] The planes of aryl-substituted arylimino groups of complexes **4** and **5** are oriented orthogonally to the plane formed by iron and the three nitrogen atoms. All structures show the disorder in the aryl groups due to "up−up" or "up−down" conformations of *o*-methyl and *o*-fluorine substituents.[4] Detailed descriptions of these conformers for each structure are shown in the captions for Figures 1−4. An interesting structural feature of **4** and **5** is that they exist mostly as "up−up" conformers in the solid state. There are no short contacts between fluoride and iron atoms in complexes **4** and **5**. The selected bond lengths of **1**, **4**, **5**, and **7** are presented in Table 1.

The axial Fe−N bonds in **4** and **5** are slightly longer than the corresponding bonds in the methyl-substituted analogue **1**. This bond elongation can be explained by the *o*-fluorine substituents being slightly larger than the *o*-hydrogens. A comparison of the bond lengths of the imino groups in **4** and **5** with those of **1** shows the same trends. The C=N bonds in **4** and **5** are slightly shorter than in **1**. It should be kept in mind, that due to the disorder, accuracies of the bond lengths are decreased. Thus, only trends are discussed here briefly.

The structure of cobalt complex **7** is generally similar to that of its iron(II) analogue **5**, except in one feature. The Co−N bonds in **7** are shorter than the corresponding Fe−N bonds in the analogous complex **5** by 0.003−0.025 Å. This shortening of metal−N bonds on going from iron(II) to cobalt(II) complexes has been described in the literature[4,8,9] and could be a reflection of the smaller van der Waals radius of Co vs. Fe.[10,11]

(4) (a) Tellmann, K. P.; Gibson, V. C.; White, A. J. P.; Williams, D. J. *Organometallics* **2005**, *24*, 280. (b) Ionkin, A. S.; Marshall, W. J.; Adelman, D. J.; Bobik Fones, B.; Fish, B. M.; Schiffhauer, M. F. *Organometallics* **2006**, *25*, 2978.

(5) (a) Small, B. L.; Brookhart, M. *Macromolecules* **1999**, *32*, 2120. (b) De Boer, E.; Johannes, M.; Deuling, H. H.; Van Der Heijden, H.; Meijboom, N.; Van Oort, A. B.; Van Zon, A. *PCT Int. Appl. WO 2001058874 A1*, 2001.

(6) (a) Mucowski, J. M.; Venuti, M. C. *J. Org. Chem.* **1980**, *45*, 4798. (b) Clark, R. D.; Mucowski, J. M.; Souchet, M.; Repke, D. B. *Synlett* **1990**, 207.

(7) Meng, D.; Parker, D. L., Jr.; Ratcliffe, R. W.; Wilkening, R. R. *PCT Int. Appl. WO 2003015761 A1*, 2003.

Scheme 3

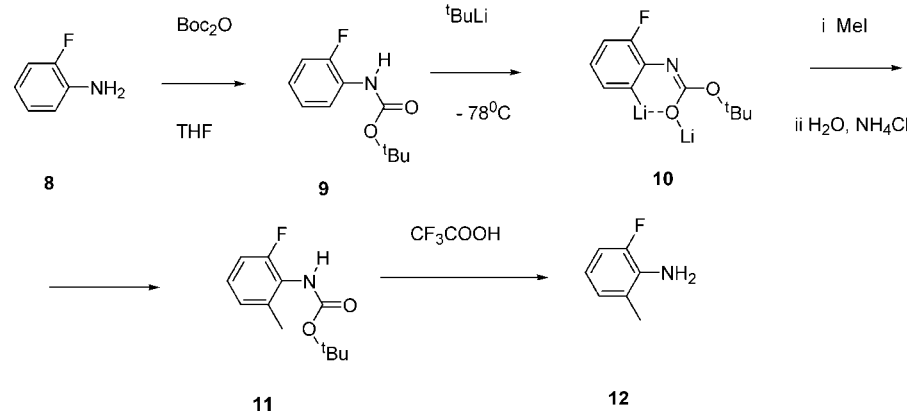

Scheme 4

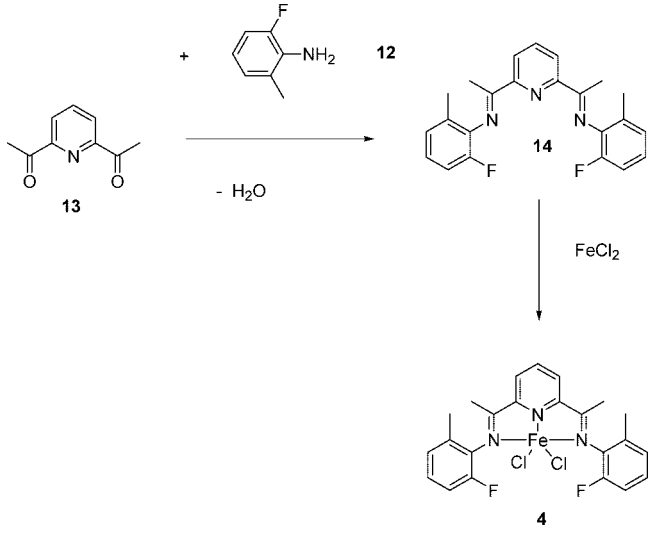

Scheme 5

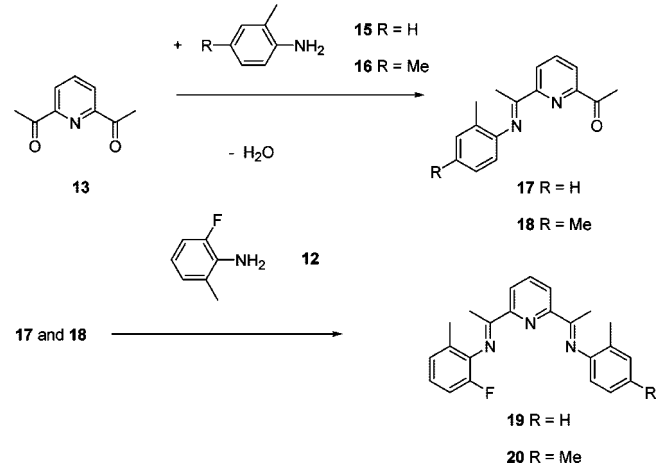

Scheme 6

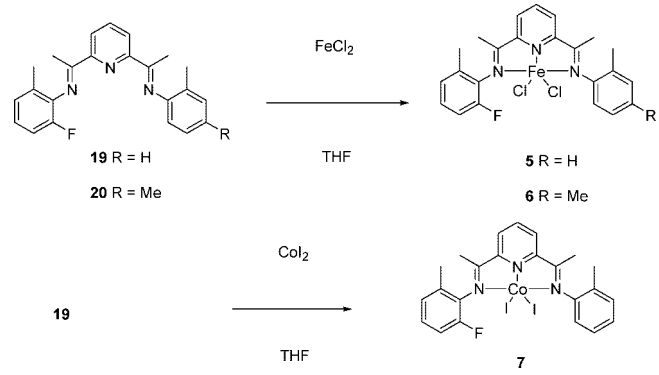

It is possible to observe ^{19}F NMR spectra of complexes **4**–**6**, however, with very broad lines associated with the paramagnetic complexes,[1] which preclude investigation of the conformeric behavior in the solution. For example, the half-width of the line of complex **4** at 30 °C in tetrachloroethane-d_2 is 1961 Hz at −89.66 ppm, and the half-width of the line of complex **4** at 110 °C is still broad at 251 Hz.

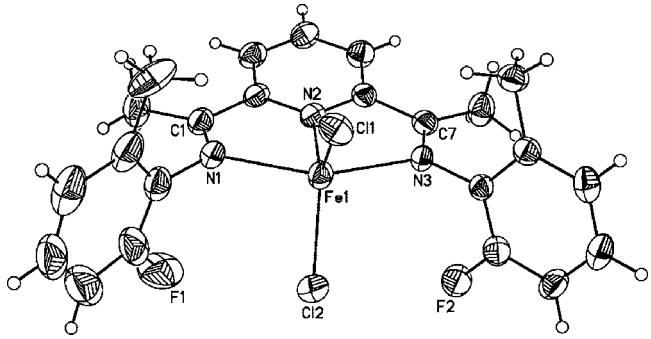

Figure 1. ORTEP drawing of {2,6-bis[1-(2-fluoro-6-methylphenylimino)ethyl]pyridine}iron(II) chloride (**4**). The crystal structure is drawn with thermal ellipsoids at the 30% probability level. The structure is displayed showing the methyl up–up disorder. The up–down or trans conformer is also present, on the basis of the occupancy refinement of the fluorine and methyl carbons and weak residual electron density peaks that could not be fully modeled. The dichloromethane solvent molecule is omitted for clarity.

Oligomerization of Ethylene to α-Olefins by the Fe(II) Dichloride Complexes 1 and 4−6. Oligomerzations were done according to the procedures given in the Experimental Section under General Conditions of the Oligomerizations. One measure of catalyst performance is its lifetime. Catalyst lifetimes were measured as the period from the beginning of ethylene uptake until flow was no longer detected by the ethylene mass flowmeter. Due to the use of this method, the lifetime of a catalyst depends on the amount of precatalyst added because

(8) Bianchini, C.; Mantovani, G.; Meli, A.; Migliacci, F.; Zanobini, F.; Laschi, F.; Sommazzi, A. *Eur. J. Inorg. Chem.* **2003**, 1620.
(9) Kooistra, T. M.; Hekking, K. F. W.; Knijnenburg, Q.; de Bruin, B.; Budzelaar, P. H.; de Gelder, R.; Smits, J. M. M.; Gal, A. W. *Eur. J. Inorg. Chem.* **2003**, 648.
(10) Long, G. J.; Clarke, P. J. *Inorg. Chem.* **1978**, *17*, 1394.
(11) Batsanov, S. S. *THEOCHEM* **1999**, *468*, 151.

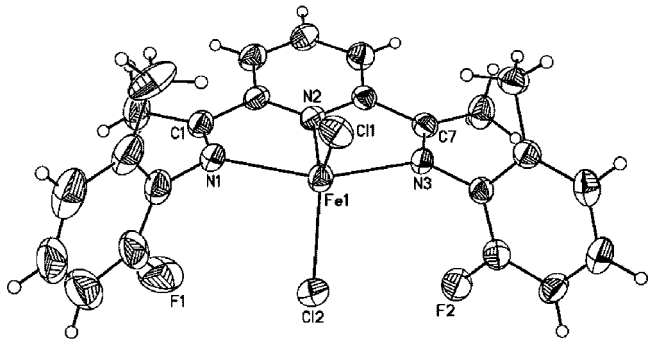

Figure 2. ORTEP drawing of {(2-fluoro-6-methylphenyl)[1-[6-(1-(*o*-tolylimino)ethyl)pyridin-2-yl]ethylidene]amine}iron(II) chloride (**5**). The crystal structure is drawn with thermal ellipsoids at the 30% probability level. The structure is always the methyl up–up conformer, on the basis of the occupancy refinement for fluorine positions and methyl carbons. The fluorine atom is disordered left to right, with F1 being as shown or near H19a in a 58/42 ratio. The dichloromethane solvent molecule is omitted for clarity.

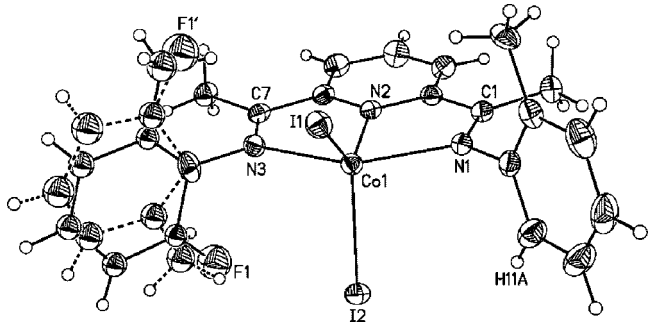

Figure 3. {(2-Fluoro-6-methylphenyl)[1-[6-(1-(*o*-tolylimino)ethyl)pyridin-2-yl]ethylidene]amine}cobalt(II) iodide (**7**). The crystal structure is drawn with thermal ellipsoids at the 30% probability level. The structure is displayed showing well resolved up–down disorder with a 53/47 ratio in favor of the up–up conformation (solid bonds). The up–down or trans conformation is shown with dashed bonds. Residual electron density near H11a suggests additional disorder that could not be fully modeled. The dichloromethane solvent molecule is omitted for clarity.

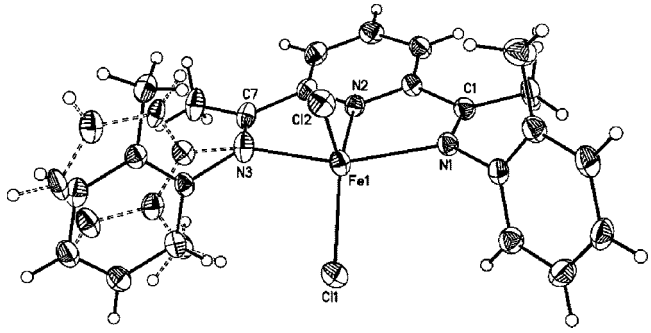

Figure 4. ORTEP drawing of {2,6-bis[1-(2-methylphenylimino)-ethyl]pyridine}iron(II) chloride (**1**). The crystal structure of **1** is drawn with thermal ellipsoids at the 50% probability level. The structure is displayed showing well resolved up–down disorder with a 72/28 ratio in favor of the up–up conformation (solid bonds). The up–down or trans conformation is shown with dashed bonds. The dichloromethane solvent molecule is omitted for clarity.

of the fixed lower detection limit of the ethylene mass flowmeter. The ethylene uptake for the remaining 10% of an initial large charge of precatalyst will still be seen, but not if the initial charge was much smaller. However, the use of a large excess of a precatalyst does not necessarily lead to an increase in lifetime, because a higher load of precatalyst can create a large exothermic effect, which greatly accelerates catalyst decomposition. This is illustrated in Figure 5, where precatalyst **1** is used at two concentrations: 0.06 and 0.43 μmol. Both runs gave similar lifetimes of about 3 min, but the productivities (kg/g) were 458 for the former and only 94 for the latter. The initial dramatic drop of ethylene pressure from 700 to 500 psig, recorded for the higher loading, shows that the oligomerization was limited by the ethylene supply. For these control reasons, the amount of precatalyst used in an experiment depended on the activity of the catalyst. Oligomerizations were repeated for a given precatalyst until the amount added did not result in an initial exothermic effect of >2 °C. Equally important, enough precatalyst was added to make an amount of α-olefins readily quantified by the analytical methods. The production of similar amounts of α-olefins in all runs gave the best possible basis for comparisons.

Ethylene uptake curves for precatalysts **1** and **4–6** are shown in Figure 6. Catalysts **1** and **4** have comparable lifetimes, as do **5** and **6**. The only clear distinguishing structural difference between the two groupings is that the former has a symmetric pattern of substitutions and the latter does not.

The results and conditions of oligomerization runs in a 1.0 L autoclave are presented in Table 2. The cobalt-based complex **7** was found to have very low activity in α-olefin oligomerization experiments within the tested temperature range of 60–130 °C and so did not make enough amounts of product for evaluation. Entries 3 and 4 in Table 2 are duplicates for precatalyst **4**. There is close agreement for all reported values across the table.

The most significant value involves the Schultz-Flory distribution constant, K. It is a measure of the molecular weight distribution of the olefins obtained and is defined as[12] $K = n(C_{n+2}\ \text{olefin})/n(C_n\ \text{olefin})$, wherein $n(C_n\ \text{olefin})$ is the number of moles of olefin containing n carbon atoms and $n(C_{n+2}\ \text{olefin})$ is the number of moles of olefin containing $n + 2$ carbon atoms, or in other words the next higher oligomer of C_n olefin. The K factor is usually preferred to be in the range of about 0.6 to about 0.8 to make α-olefins of the most commercial interest. It is also desirable to be able to vary this factor to make a range of products.

As seen in Table 2, precatalysts **4–6** gave α-olefins with K values above 0.6, which make them attractive from a commercial point of view. The α-olefins with K values below 0.6 are richer in butenes, which have minimal commercial value. The value of K changes significantly as a function of precatalyst structure.

A possible explanation could involve the different number of fluorines present in the precatalysts. The K value drops with the number of fluorines in the structures. For the 120 °C runs, precatalyst **4** has two fluorines and a K value of 0.72 and precatalyst **1** has no fluorines and the lowest K value of 0.59. This would suggest that more steric hindrance around the active catalytic center increases the ratio of propagation to termination/transfer rates to raise K values. This is the normal dependency for the Versipol family of catalysts.[1] An increase of the steric bulk around iron usually leads to an increase in the K value.[8,13]

Referring again to Table 2, the percent solids of total LAO are the percentages of α-olefins with >C28 chain lengths. Since some of these will precipitate from the carrier solvent, *o*-xylene, it is desirable to run oligomerizations at temperatures as high

(12) Elvers, B., et al., Ed. *Ullmann's Encyclopedia of Industrial Chemistry*; VCH: Weinheim, Germany, 1989; Vol. A13, pp 243–247 and 275−276.

Table 1. Selected Bond Lengths (Å) for 1, 4, 5, and 7

	1	4	5	7
axial (imino) N−M	2.2303(16) (Fe−N1)	2.247(3) (Fe−N1)	2.235(2) (Fe−N1, aryl-F side)	2.232(3) (Co−N3, aryl-F side)
axial (imino) N−M	2.2424(17) (Fe−N3)	2.244(3) (Fe−N3)	2.230(2) (Fe−N3)	2.205(3) (Co−N1)
basal (central) N−M	2.0943(16) (Fe−N2)	2.108(3) (Fe−N2)	2.106(2) (Fe−N2)	2.031(3) (Co−N2)
C=N	1.281(2) (N1−C1)	1.274(5) (N1−C1)	1.279(4) (N1−C1, aryl-F side)	1.278(5) (N3−C7, aryl-F side)
C=N	1.287(3) (N3−C7)	1.281(5) (N3−C7)	1.280(4) (N3−C7)	1.276(5) (N1−C1)

as 120 °C to keep more of these in solution to delay system plugging and to use a catalyst, which minimizes their formation for a given product distribution. A catalyst which makes a distribution with a high-molecular-weight tail on an otherwise normally distributed product would be undesirable. Looking at the solids' data in Table 2, there is no clear trend for solids vs. any of the variables listed for the 120 °C oligomerizations or as a function of structural differences.

The productivities of the precatalysts are also given in Table 2. At 120 °C, precatalysts **4**–**6** have productivities that are less than the average value for **1**. While the relative differences are not as great here as they were for the argument above concerning K values and the effect of steric hindrance at the active center, the same trend is seen here. The highest productivity is seen for **1**, which has only two ortho substituents, and the lowest is seen for **4**, which has four. The productivities for precatalysts **5** and **6** with three substituents are nearly comparable to each other but fall between those of **1** and **4**. This indicates that an increase in steric hindrance in the ortho positions slows access of ethylene to the metal center of the catalyst.

In Table 2 is a list of productivities for precatalyst **4** as a function of temperature. There is a clear trend of a decrease in productivity with increasing temperature. Provided the diffusion of ethylene to the active centers was not limiting, this suggests that catalyst decomposition is a much stronger function of temperature than is propagation. Interestingly, the constant K value over this temperature interval suggests that the ratio of propagation to termination rates did not change.

The right-hand column of Table 2 is a list of the correlation coefficients (SFD R^2) for the goodness of fit of the Schultz−Flory distribution equation to the experimental data. Ideally, a catalyst will make α-olefins which fit the Schultz−Flory distribution equation. One measure of the approach to ideality comes from plotting $\ln(m_p/D_p)$ vs. $D_p - 2$ according to the equation $\ln(m_p/D_p) = \ln((1 - K)^2/(2 - K)) + (D_p - 2) \ln K$, where m_p is the

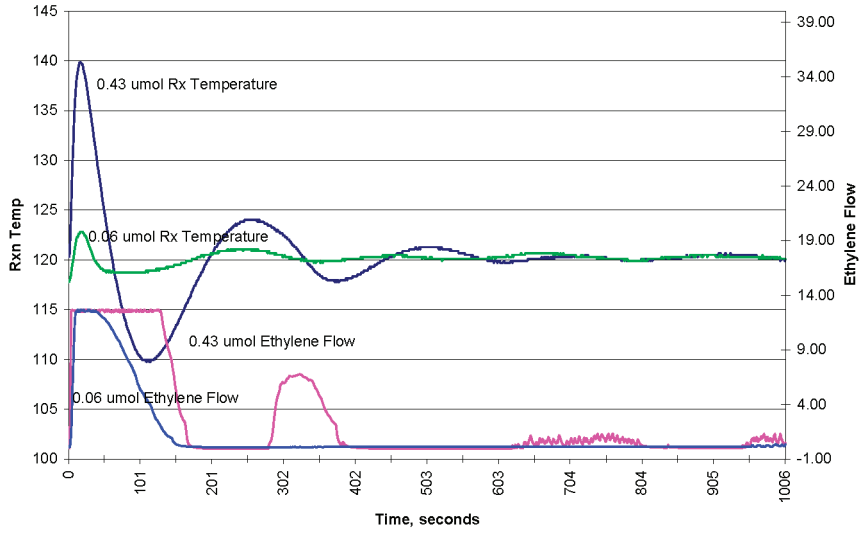

Figure 5. Effect of the concentrations of parent precatalyst **1** on the temperature and ethylene flow.

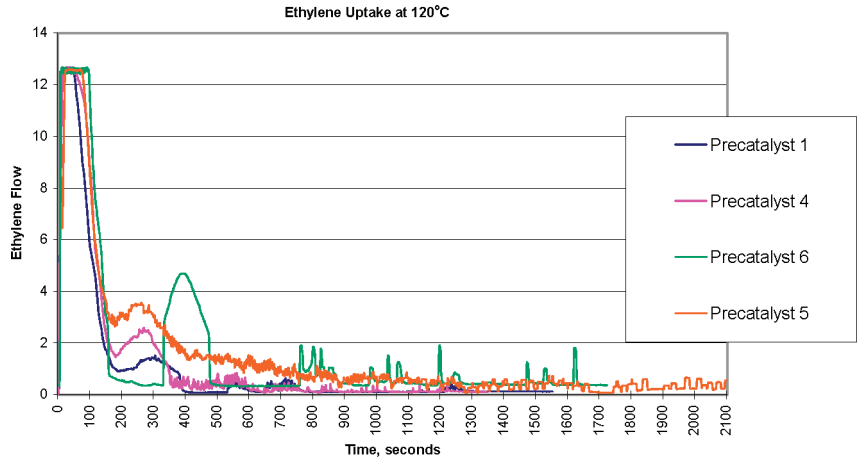

Figure 6. Graph of ethylene uptake of complexes **1** and **4**−**6** in the catalytic oligomerization of ethylene.

Table 2. α-Olefins from Ethylene Oligomerizations by Iron(II) Complexes 1 and 4−6[a]

entry	precat. (amt, μmol)	amt of cocat. MMAO, mmol	temp, °C	*K* value Schultz−Flory distribn[b]	kg of LAO/g of cat.	solids of total LAO, %[c]	SFD R^2
1	**4** (0.10)	2.26	135	0.71	19	9.72	0.9831
2	**4** (0.20)	2.26	125	0.72	155	4.76	0.9976
3	**4** (0.16)	2.26	120	0.72	247	6.05	0.9934
4	**4** (0.10)	2.26	120	0.72	246	5.44	0.9963
5	**5** (0.21)	2.26	120	0.61	263	3.43	0.9974
6	**6** (0.20)	2.26	120	0.62	278	7.71	0.9973
7	**1** (0.06)	1.13	120	0.59	458	3.44	0.9862

[a] Conditions: solvent *o*-xylene, 600 mL; pressure, 700 psig. [b] Determined from GC, using extrapolated values for C-10 and C-12. [c] Xylene-insoluble fraction of α-olefins.

Table 3. Summary of Crystal Data, Data Collection, and Structural Refinement Parameters for 1, 4, 5, and 7

	1	**4**	**5**	**7**
empirical formula	$C_{24}H_{25}Cl_4FeN_3$	$C_{24}H_{23}Cl_4F_2FeN_3$	$C_{24}H_{24}Cl_4FeN_3F$	$C_{24}H_{24}Cl_2CoI_2N_3F$
fw	553.12	589.1	571.11	757.09
cryst color, form	blue, needle	blue, rect. plate	black, needle	red, prism
cryst syst	monoclinic	monoclinic	monoclinic	monoclinic
space group	$P2_1/c$	$I2/a$	$C2/c$	$P2_1/n$
a (Å)	10.4140(5)	15.867(5)	25.6657(10)	13.3251(11)
b (Å)	15.2465(8)	15.220(5)	15.2699(6)	14.5228(12)
c (Å)	15.8488(8)	21.709(7)	15.7230(6)	14.7832(12)
α (deg)	90	90	90	90
β (deg)	92.3650(10)	93.565(6)	122.9210(10	107.9410(10
γ (deg)	90	90	90	90
V (Å^3)	2514.3(2)	5232(3)	5172.5(3)	2721.7(4)
Z	4	8	8	4
density (g/cm^3)	1.461	1.496	1.467	1.848
abs μ (mm^{-1})	1.042	1.017	1.021	3.12
F(000)	1136	2400	2336	1460
cryst size (mm)	0.320 × 0.060 × 0.020	0.500 × 0.120 × 0.020	0.400 × 0.050 × 0.010	0.250 × 0.130 × 0.130
temp (°C)	−100	−100	−100	−100
scan mode	ω	ω	ω	ω
detector	Bruker-CCD	Bruker-CCD	Bruker-CCD	Bruker-CCD
θ_{max} (deg)	27.96	27.27	28.43	30.44
no. of obsd rflns	37 670	22 010	22 038	52 377
no. of unique rflns	6038	5845	6456	8056
R_{merge}	0.055	0.065	0.049	0.047
no. params	358	315	313	298
S[b]	1.02	1.04	1.06	1.06
R indices ($I > 2\sigma(I)$)[a]	wR2 = 0.075, R1 = 0.036	wR2 = 0.142, R1 = 0.059	wR2 = 0.123, R1 = 0.051	wR2 = 0.095, R1 = 0.038
R indices (all data)[a]	wR2 = 0.084, R1 = 0.060	wR2 = 0.166, R1 = 0.097	wR2 = 0.140, R1 = 0.086	wR2 = 0.104, R1 = 0.059
max diff peak, hole (e/Å^3)	0.288, −0.325	1.189, −0.824	0.888, −0.647	1.931, −0.899

[a] $R1 = \sum||F_o| - |F_c||/\sum|F_o|$; $wR2 = \{\sum[w(F_o^2 - F_c^2)^2]/\sum[w(F_o^2)^2]\}^{1/2}$ (sometimes denoted as R_w^2). [b] $GOF = S = \{\sum[w(F_o^2 - F_c^2)^2]/(n - p)\}^{1/2}$, where *n* is the number of reflections and *p* is the total number of refined parameters.

weight fraction of the α-olefin, D_p is the degree of polymerization of the α-olefin, and *K* is the Schultz−Flory distribution factor.

The R^2 values for plots of experimental data according to the above equation are given in Table 3. There are no obvious trends. Possibly a clearer way to see that there are differences in deviations from ideality, especially at the low-molecular-weight end of the distribution, is achieved by plotting ideal distributions with the experimental data. Several such plots are shown in Figures 7−9. The solid lines are the ideal Schultz−Flory product distributions predicted for the specified *K* factor, and the symbols are the experimental data points. The magnitudes of the deviations of the data points from their respective solid lines are an indication of the ideality of the catalyst performance. Precatalyst **1** generally shows a larger deviation at the low carbon number end in Figures 7−9 than do the other precatalysts. This means catalyst **1** makes more C6 and C8 products than do the other catalysts and so has a less ideal product distribution.

To summarize, the new Fe-based bis(imino)pyridine complexes **4**–**6** and Co-based bis(imino)pyridine complex **7**, functionalized with double patterns of substitutions, *o*-methyl plus *o*-fluorine in the same imino arm, were synthesized and fully characterized. The Fe-based bis(imino)pyridine complexes **4**–**6** afforded very active catalysts for the production of α-olefins with more ideal Schultz−Flory distributions of α-olefins and with higher *K* values than the parent methyl-substituted Fe(II) complex **1**. The cobalt complex **7** was found to have very low activity in the oligomerization experiments, which is in agreement with the low activity of such cobalt complexes.[1] On the basis of limited observations, it appears the nonsymmetric precatalysts **5** and **6** had longer lifetimes than the symmetric precatalysts **1** and **4**. Steric hindrance around the active center, in terms of the number of ortho substituents, appears to affect the product distributions and catalyst productivities. More steric hindrance seems to shift the distributions to longer chain α-olefins but reduces the productivities.

Judging from all of these criteria, the complex **5** was found to be the best catalyst for high temperature production of α-olefins in this study.

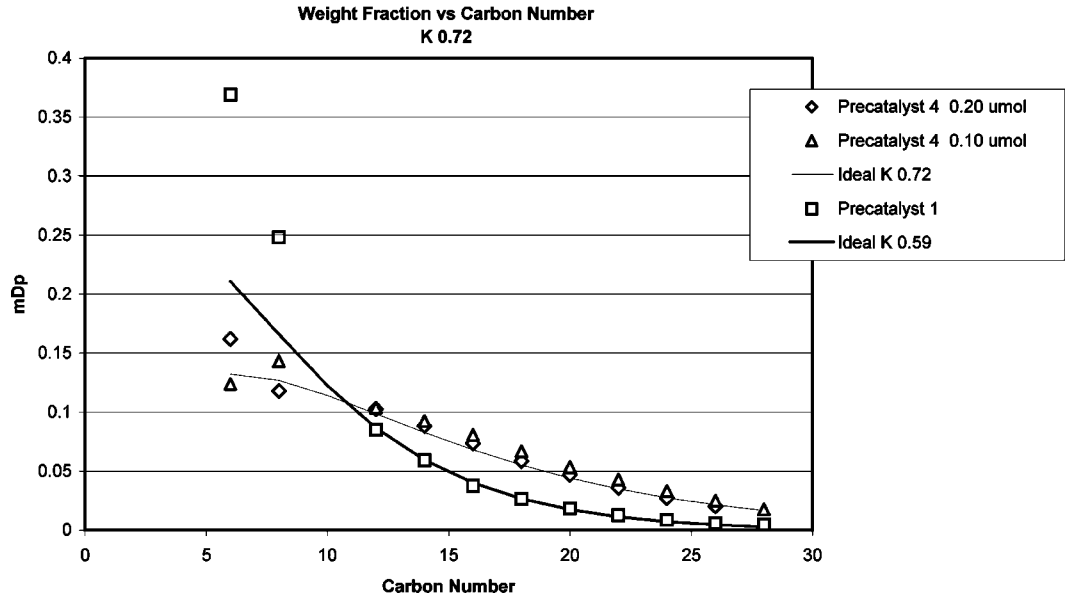

Figure 7. Distribution of α-olefins from C-2 to C-28 for precatalysts **1** and **4** and ideal Schultz−Flory distributions with *K* factors at 0.59 and 0.72.

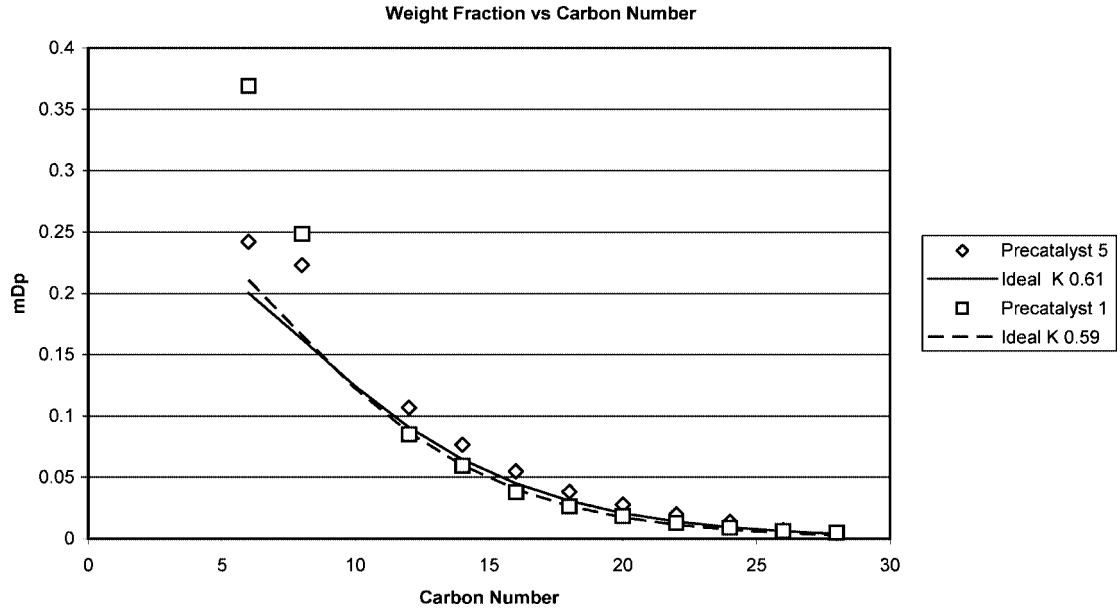

Figure 8. Distribution of α-olefins from C-2 to C-28 for precatalysts **1** and **5** and ideal Schultz−Flory distribution with *K* factors at 0.59 and 0.61.

Experimental Section

All air-sensitive compounds were prepared and handled under a N_2/Ar atmosphere using standard Schlenk and inert-atmosphere box techniques. Anhydrous solvents were used in the reactions. Solvents were distilled from drying agents or passed through columns under an argon or nitrogen atmosphere. Anhydrous iron(II) chloride, 1-(6-acetylpyridin-2-yl)ethanone, 2-fluorophenylamine, di-*tert*-butyl dicarbonate, 1.7 M *tert*-butyllithium in pentane, iodomethane, 2,4-dimethylphenylamine, *o*-tolylamine, and *n*-butanol were purchased from Aldrich. MMAO was purchased from Akzo-Nobel. Complex **1** was prepared according to the literature.[14]

***tert*-Butyl 2-Fluorophenyl Carbamate (9).** A 50 g (0.450 mol) amount of 2-fluorophenylamine (**8**) was mixed in 500 mL of dry THF. To this was added 100 g (0.458 mol) of di-*tert*-butyl dicarbonate. This mixture was then stirred under a nitrogen atmosphere and heated in a water bath to 60 °C for 3 days. The solution was extracted with ethyl acetate, and the organic fraction was then washed three times with 1 M citric acid and left overnight to dry over magnesium sulfate. The solvent was then removed and the crude product was dissolved in hexane. This solution was then filtered over Celite to remove the solids and the solvent removed to leave a yellow liquid. Further purification was achieved through distillation; the cleanest fractions came off as a 54–57 °C vapor at 20×10^{-3} mm Hg to form a viscous clear liquid. The yield of **9**

(13) Britovsek, G. J. P.; Gibson, V. C.; Mastroianni, S.; Oakes, D. C. H.; Redshaw, C.; Solan, G. A.; White, A. J. P.; Williams, D. J. *Eur. J. Inorg. Chem.* **2001**, *2*, 431.

(14) Small, B. L.; Brookhart, M.; Bennett, A. M. A. *J. Am. Chem. Soc.* **1998**, *120*, 4049.

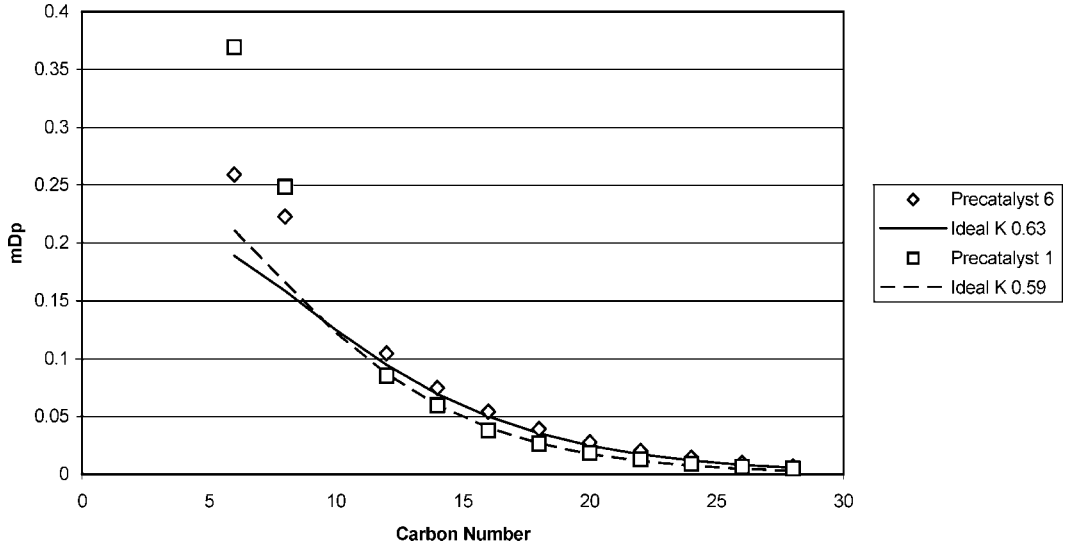

Figure 9. Distribution of α-olefins from C-2 to C-28 for precatalysts **1** and **6** and ideal Schultz−Flory distribution with *K* factors at 0.59 and 0.63.

was 74.1 g (78%). ^{1}H NMR (500 MHz, C_6D_6, TMS): δ 1.40 (s, 9 H, Me), 6.65–6.80 (m, 4H, arom H), 8.40 (br, 1H, N−H). ^{19}F NMR (500 MHz, C_6D_6): δ −136.5 (br, 1F).

***tert*-Butyl 2-Fluoro-6-methylphenyl Carbamate (11).** A 20 g (0.095 mol) amount of *tert*-butyl 2-fluorophenyl carbamate (**9**) was dissolved in 200 mL of dry THF and cooled to −78 °C. Once the mixture was cooled, 139 mL of 1.7 M *tert*-butyllithium in pentane solution was added. The mixture was then warmed to −15 °C over a 2 h period. At that point it was cooled back down to −78 °C and 6.47 mL of iodomethane was added slowly. The mixture was then warmed to 0 °C, and 20 mL of saturated ammonium chloride solution was added slowly. The mixture was then extracted with ethyl acetate and washed with water three times. The solution was dried over magnesium sulfate overnight. It was then filtered, and the solvent was removed by vacuum. The precipitate from the residue was filtered off and washed with petroleum ether to leave a white powder. The yield of **11** was 14.60 g (68%). ^{1}H NMR (500 MHz, C_6D_6, TMS): δ 1.45 (s, 9 H, Me), 2.35 (s, 3H, Me), 6.10 (br, 1H, N−H), 6.80 (m, 1H, arom H), 6.90 (m, 1H, arom H), 7.00 (m, 1H, arom H). ^{19}F NMR (500 MHz, C_6D_6): δ − 128.0 (br, 1F).

2-Fluoro-6-methylphenylamine (12). A solution of 7 g (0.031 mol) of *tert*-butyl 2-fluoro-6-methylphenyl carbamate (**11**) in 30 mL of trifluoroacetic acid was stirred for 1 h. The excess trifluoroacetic acid was removed under vacuum, and the residue was diluted with methylene chloride. This was then poured into a slurry of sodium carbonate and methylene chloride, additional sodium carbonate was added as needed, and the mixture was stirred for 1 h. This solution was filtered and the solvent removed. The residue was then distilled, and the desired fraction came off as a 63 °C vapor at 15 mbar and crystallized as an off-white solid. The yield of **12** was 2.47 g (64%). ^{1}H NMR (500 MHz, C_6D_6, TMS): δ 1.60 (s, 3 H, Me), 3.00 (br, 2H, N−H), 6.40 (m, 1H, arom H), 6.60 (m, 1H, arom H), 6.80 (m, 1H, arom H). ^{19}F NMR (500 MHz, C_6D_6): δ −137.1 (s, 1F).

2,6-Bis{1-[(2-fluoro-6-methylphenyl)imino]ethyl}pyridine (14). A 1.1 g amount (0.0068 mol) of 1-(6-acetylpyridin-2-yl)ethanone (**13**), 1.7 g (0.0136 mol) of 2-fluoro-6-methylphenylamine (**12**), 100 mL of toluene, and 100 g of fresh molecular sieves were kept at 100 °C for 3 days. The molecular sieves were removed by filtration. The solvent was removed in a rotary evaporator, and the residue was recrystallized from 20 mL of ethanol. The yield of 2,6-bis{1-[(2-fluoro-6-methylphenyl)imino]ethyl}pyridine (**14**) was 1.78 g (70%) as a pale yellow solid. ^{1}H NMR (500 MHz, C_6D_6, TMS): δ 2.05 (s, 6 H, Me), 2.36 (s, 6 H, Me), 6.60–6.90 (m, 6H, arom H), 7.20 (t, $^3J_{HH}$ = 7.8 Hz, 1H, Py H), 8.40 (d, $^3J_{HH}$ = 7.8 Hz, 2H, Py H). ^{19}F NMR (500 MHz, C_6D_6): δ −127.7 (br, 2F). ^{13}C NMR (500 MHz, C_6D_6 (selected signals)): δ 169.6 (C═N). Anal. Calcd for $C_{23}H_{21}F_2N_3$ (mol wt 377.43): C, 73.19; H, 5.61; N, 11.13. Found: C, 73.42; H, 5.68; N, 11.38.

{2,6-Bis[1-((2-fluoro-6-methylphenyl)imino)ethyl]pyridine}-iron(II) Chloride (4). 0.94 g (0.0025 mol) of 2,6-Bis(1-(2-fluoro-6-methylphenylimino)ethyl)pyridine (**14**) was dissolved in 30 mL of THF. 0.30 g (0.0024 mol) of Iron(II) chloride was added in the reaction mixture by one portion. The resultant blue precipitate was filtered after 12 h of stirring, washed twice by 20 mL of pentane, and dried at 1-mm vacuum. Yield of 2,6-bis(1-(2-fluoro-6-methylphenylimino)ethyl)pyridineiron(II) chloride (**4**) was 3.19 g (48%). Anal. Calculated for $C_{23}H_{21}Cl_2F_2FeN_3$ (Mol. Wt.: 504.18): C, 54.79; H, 4.20; N, 8.33. Found: C, 55.03; H, 4.37; N, 8.40. The structure was determined by X-ray analysis. A crystal suitable for X-ray analysis was grown from methylene chloride.

1-{6-[1-(*o*-Tolylimino)ethyl]pyridin-2-yl}ethanone (17). A 57.11 g amount (0.35 mol) of 1-(6-acetylpyridin-2-yl)ethanone (**13**), 25.0 g (0.23 mol) of *o*-tolylamine (**15**), 200 mL of methanol, and a few crystals of *p*-toluenesulfonic acid were stirred at room temperature for 36 h in 1.0 L flask under a flow of nitrogen. The resultant yellow precipitate was filtered and washed with 20 mL of methanol. It was then dried under 1 mm vacuum overnight. The yield of 1-{6-[1-(*o*-tolylimino)ethyl]pyridin-2-yl}ethanone (**17**) was 8.13 g (14%) as a yellow solid. ^{1}H NMR (500 MHz, CD_2Cl_2, TMS): δ 2.00 (s, 3 H, Me), 2.20 (s, 3 H, Me), 2.65 (s, 3 H, Me), 6.55 (m, 1H, arom H), 6.90 (m, 1H, arom H), 7.10 (m, 2H, arom H), 7.70 (t, $^3J_{HH}$ = 8.0 Hz, 1H, Py H), 7.90 (d, $^3J_{HH}$ = 8.0 Hz, 1H, Py H), 8.45 (d, $^3J_{HH}$ = 8.0 Hz, 1H, Py H). ^{13}C NMR (500 MHz, CD_2Cl_2, TMS (selected signals)): δ 166.6 (C═N), 200.1 (C═O). Anal. Calcd for $C_{16}H_{16}N_2O$ (mol wt 252.31): C, 76.16; H, 6.39; N, 11.10. Found: C, 76.24; H, 6.46; N, 11.36.

(2-Fluoro-6-methylphenyl){1-[6-(1-(*o*-tolylimino)ethyl)pyridin-2-yl]ethylidene}amine (19). A 6.05 g amount (0.024 mol) of 1-{6-[1-(*o*-tolylimino)ethyl]pyridin-2-yl}ethanone (**17**), 2.5 g (0.01997 mol) of 2-fluoro-6-methylphenylamine (**12**), 100 mL of toluene, and 100 g of fresh molecular sieves were kept at 100 °C for 3 days. The molecular sieves were removed by filtration. The solvent was removed in a rotary evaporator, and the residue was recrystallized from 20 mL of ethanol. The yield of (2-fluoro-6-methylphenyl){1-[6-(1-(*o*-tolylimino)ethyl)pyridin-2-yl]ethyl-

idene}amine (**19**) was 6.98 g (81%) as a pale yellow solid. ^{1}H NMR (500 MHz, CD_2Cl_2, TMS): δ 2.10 (s, 3 H, Me), 2.15 (s, 3 H, Me), 2.30 (s, 3 H, Me), 2.35 (s, 3 H, Me), 6.60 (m, 1H, arom H), 6.90–7.15 (m, 6H, arom H), 7.90 (m, 1H, Py H), 8.40 (m, 2H, Py H). ^{19}F NMR (500 MHz, C_6D_6): δ −128.7 (br, 1F). ^{13}C NMR (500 MHz, C_6D_6 (selected signals)): δ 170.2 (C═N), 167.3 (C═N). Anal. Calcd for $C_{23}H_{22}FN_3$ (mol wt 359.44): C, 76.85; H, 6.17; N, 11.69. Found: C, 77.02; H, 6.31; N, 11.83.

{(2-Fluoro-6-methylphenyl)[1-[6-(1-(*o*-tolylimino)ethyl)pyridin-2-yl]ethylidene]amine}iron(II) Chloride (5). A 2.00 g amount (0.00556 mol) of (2-fluoro-6-methylphenyl){1-[6-(1-(*o*-tolylimino)ethyl)pyridin-2-yl]ethylidene}amine (**19**) was dissolved in 30 mL of THF. A 0.63 g amount (0.0050 mol) of iron(II) chloride was added to the reaction mixture in one portion. The resultant blue precipitate was filtered after 12 h of stirring, washed twice with 20 mL of pentane, and dried under 1 mm vacuum. The yield of {(2-fluoro-6-methylphenyl)[1-[6-(1-(*o*-tolylimino)ethyl)pyridin-2-yl]ethylidene]amine}iron(II) chloride (**5**) was 2.13 g (88%). Anal. Calcd for $C_{23}H_{22}Cl_2FFeN_3$ (mol wt 486.19): C, 56.82; H, 4.56; N, 8.64. Found: C, 56.94; H, 4.63; N, 8.69. The structure was determined by X-ray analysis. A crystal suitable for X-ray analysis was grown from methylene chloride.

1-{6-[1-((2,4-Dimethylphenyl)imino)ethyl]pyridin-2-yl}ethanone (18). A 37.0 g amount (0.23 mol) of 1-(6-acetylpyridin-2-yl)ethanone (**13**), 25.0 g (0.21 mol) of 2,4-dimethylphenylamine (**16**), 300 mL of *n*-propanol, and a few crystals of *p*-toluenesulfonic acid were stirred at room temperature for 36 h in a 1.0 L flask under a flow of nitrogen. The resultant yellow precipitate was filtered and washed with 20 mL of methanol. It was then dried under 1 mm vacuum overnight. The yield of 1-{6-[1-((2,4-dimethylphenyl)imino)ethyl]pyridin-2-yl}ethanone (**18**) was 11.20 g (21%) as a yellow solid. ^{1}H NMR (500 MHz, Tol-d_8, TMS): δ 2.10 (s, 6 H, Me), 2.20 (s, 3 H, Me), 2.25 (s, 3 H, Me), 2.56 (s, 3 H, Me), 6.50 (m, 1H, arom H), 6.90 (m, 2H, arom H), 7.40 (t, $^3J_{HH}$ = 8.0 Hz, 1H, Py H), 7.90 (d, $^3J_{HH}$ = 8.0 Hz, 1H, Py H), 8.45 (d, $^3J_{HH}$ = 8.0 Hz, 1H, Py H). ^{13}C NMR (500 MHz, CD_2Cl_2, TMS (selected signals)): δ 162.2 (C═N), 198.7 (C═O). Anal. Calcd for $C_{17}H_{18}N_2O$ (mol wt 266.34): C, 76.66; H, 6.81; N, 10.52. Found: C, 76.73; H, 7.03; N, 10.70.

{1-[6-[1-((2-Fluoro-6-methylphenyl)imino)ethyl]pyridin-2-yl]-ethylidene}(2,4-dimethylphenyl)amine (20). A 5.00 g amount (0.0187 mol) of 1-{6-[1-((2,4-dimethylphenyl)imino)ethyl]pyridin-2-yl}ethanone (**18**), 2.82 g (0.023 mol) of 2-fluoro-6-methylphenylamine (**12**), 100 mL of toluene, and 100 g of fresh molecular sieves were kept at 100 °C for 3 days. The molecular sieves were removed by filtration. The solvent was removed in a rotary evaporator, and the residue was recrystallized from 20 mL of ethanol. The yield of {1-[6-[1-((2-fluoro-6-methylphenyl)imino)ethyl]pyridin-2-yl]ethylidene}(2,4-dimethylphenyl)-amine (**20**) was 5.47 g (78%) as a pale yellow solid. ^{1}H NMR (500 MHz, C_6D_6, TMS): δ 1.90 (s, 3 H, Me), 1.95 (s, 3 H, Me), 2.10 (s, 3 H, Me), 2.20 (s, 3 H, Me), 2.30 (s, 3 H, Me), 6.45 (m, 1H, arom H), 6.60–6.90 (m, 5H, arom H), 7.10 (m, 1H, Py H), 8.30 (m, 2H, Py H). ^{19}F NMR (500 MHz, C_6D_6): δ −127.6 (br, 1F). ^{13}C NMR (500 MHz, C_6D_6 (selected signals)): δ 169.4 (C═N), 166.5 (C═N). Anal. Calcd for $C_{24}H_{24}FN_3$ (mol wt 373.47): C, 77.18; H, 6.48; N, 11.25. Found: C, 77.19; H, 6.53; N, 11.28.

{[1-[6-[1-((2-Fluoro-6-methylphenyl)imino)ethyl]pyridin-2-yl]-ethylidene](2,4-dimethylphenyl)amine}iron(II) Chloride (6). A 2.14 g amount (0.00573 mol) of {1-[6-[1-((2-fluoro-6-methylphenyl)imino)ethyl]pyridin-2-yl]ethylidene}(2,4-dimethylphenyl)-amine (**20**) was dissolved in 40 mL of THF. A 0.69 g amount (0.0054 mol) of iron(II) chloride was added to the reaction mixture in one portion. The resultant blue precipitate was filtered after 12 h of stirring, washed twice with 20 mL of pentane, and dried under 1 mm vacuum. The yield of {[1-[6-[1-((2-fluoro-6-methylphenyl)-imino)ethyl]pyridin-2-yl]ethylidene](2,4-dimethylphenyl)amine}-iron(II) chloride (**6**) was 2.48 g (91%). Anal. Calcd for $C_{24}H_{24}Cl_2FFeN_3$ (mol wt 500.22): C, 57.63; H, 4.84; N, 8.40. Found: C, 57.73; H, 5.01; N, 8.52. The structure was determined by X-ray analysis. A crystal suitable for X-ray analysis was grown from methylene chloride.

{(2-Fluoro-6-methylphenyl)[1-[6-(1-(*o*-tolylimino)ethyl)pyridin-2-yl]ethylidene]amine}cobalt(II) Iodide (7). A 1.00 g amount (0.00278 mol) of (2-fluoro-6-methylphenyl){1-[6-(1-(*o*-tolylimino)ethyl)pyridin-2-yl]ethylidene}amine (**19**) was dissolved in 30 mL of THF. A 0.78 g amount (0.0025 mol) of cobalt(II) iodide was added to the reaction mixture in one portion. The resultant brown precipitate was filtered after 12 h of stirring, washed twice with 20 mL of pentane, and dried under 1 mm vacuum. The yield of {(2-fluoro-6-methylphenyl)[1-[6-(1-(*o*-tolylimino)ethyl)pyridin-2-yl]ethylidene]amine}cobalt(II) iodide (**7**) was 1.19 g (71%). Anal. Calcd for $C_{23}H_{22}CoFI_2N_3$ (mol wt 672.18): C, 41.10; H, 3.30; N, 6.25. Found: C, 41.29; H, 3.42; N, 6.37. The structure was determined by X-ray analysis. A crystal suitable for X-ray analysis was grown from methylene chloride.

General Conditions of the Oligomerizations. Ethylene oligomerizations were done in a 1 L 316 stainless steel Autoclave Engineers Zipperclave. The catalyst and cocatalyst were charged separately using stainless steel injection tubes. The complexes **1** and **4**−**7** were activated by modified methylaluminoxane (MMAO). The steps for a typical oligomerization are as follows. The injectors were charged in a glovebox. The cocatalyst was obtained as a 7 wt % solution in *o*-xylene and was charged as such into the injector assembly along with a 10 mL chase of *o*-xylene. The catalysts were prepared as suspensions in *o*-xylene (10 mg/100 mL). A sample was pulled from a well-stirred suspension and was added to a 10 mL charge of *o*-xylene. The injectors were attached to autoclave ports equipped with dip tubes. Nitrogen was sparged through the loose fittings at the attachment points prior to making them tight. The desired charge of *o*-xylene (600 mL was the usual amount) was then pressured into the autoclave. The agitator (1000 rpm) and heater were turned on. When the desired temperature was reached, the cocatalyst was charged into the clave by blowing ethylene down through the cocatalyst injector. After a significant pressure rise was seen in the autoclave to indicate the cocatalyst and chase solvent had entered, the injector was isolated from the process using its valves. The pressure controller was then set to 5 psig below the desired ethylene operating pressure and was put in the automatic mode to allow it to control the operation of the ethylene addition valve. When the pressure was 5 psig below the desired operating pressure, the controller was put into manual mode and the valve was set to 0% output. When the batch temperature was stable at the desired value, the catalyst was injected using enough nitrogen such that the reactor pressure was boosted to the desired pressure. At the same time as the catalyst injection, the pressure controller was put in the automatic mode and the oligomerization was underway. The 5 psi boost was obtained routinely by having a small reservoir between the nitrogen source and the catalyst injector. A valve was closed between the nitrogen source and the reservoir prior to injecting the catalyst so that the same volume of nitrogen was used each time to inject the catalyst suspension. To stop the oligomerization, the pressure controller was put into manual, the ethylene valve was closed, and the reactor was cooled. The reaction time was 1 h.

X-ray Diffraction Studies. Data for all structures were collected using a Bruker CCD system at −100 °C. Structure solution

and refinement were performed using the Shelxtl[15] set of programs. The Platon-Squeeze[16] program was used to correct the data where the solvent molecules could not be correctly modeled. A summary of crystal data and data collection and structural refinement parameters for **1**, **4**, **5**, and **7** is given in Table 3.

Acknowledgment. We wish to thank Kurt Adams for funding X-ray research.

Supporting Information Available: CIF files for compounds **1**, **4**, **5**, and **7**. This material is available free of charge via the Internet at http://pubs.acs.org.

OM701204W

(15) Sheldrick, G. Shelxtl Software Suite, Version 5.1; Bruker AXS Corp., Madison, WI.

(16) Spek, A. L. PLATON, A Multipurpose Crystallographic Tool; Utrecht University, Utrecht, The Netherlands, 2005.